Self-Powered Multi-Input Serial SSHI Interface Circuit With Arbitrary Phase Difference for Piezoelectric Energy Harvesting

Zhidong Chen, Yinshui Xia, *Member, IEEE*, Ge Shi, Xiudeng Wang, *Student Member, IEEE*, Huakang Xia, and Yidie Ye, *Member, IEEE*

***Abstract*—A self-powered multi-input serial synchronized switch harvesting on inductor (MIS-SSHI) interface circuit with arbitrary phase difference for piezoelectric energy harvesting is proposed in this article. The proposed MIS-SSHI can extract energy from multiple PZTs based on S-SSHI technique and handle inductor access conflict to avoid mutual influence between the PZTs, without using extra inductor access controlling circuit. Four cases of different phases between PZTs are discussed to explain how to handle the inductor access conflict. Besides, the diodes in traditional S-SSHI circuit are removed to improve the conversion efficiency. An experimental platform is built for testing the power generation performance of the proposed circuit. The experimental results show that the proposed MIS-SSHI circuit can harvest energy from two PZTs with arbitrary phase difference (0-2π) based on single inductor. The maximum harvested power of the proposed MIS-SSHI circuit for single PZT can reach 3.7 times that of the standard energy harvesting circuit.**

***Index Terms*—Energy harvesting, multi-input, piezoelectric, PZT, serial SSHI.**

I. Introduction

STRUCTURED by a certain number of autonomous sensor nodes, the wireless sensor networks (WSNs) can be used for monitoring different physical condition and environment information [1], [2]. However, powering these ubiquitous WSNs nodes and making them fully self-sustained remain a key challenge [3]. Fortunately, energy harvesting (EH) is expected to meet the demands by harvesting ambient energy and converting it into electricity for powering the WSNs nodes [4], [5].

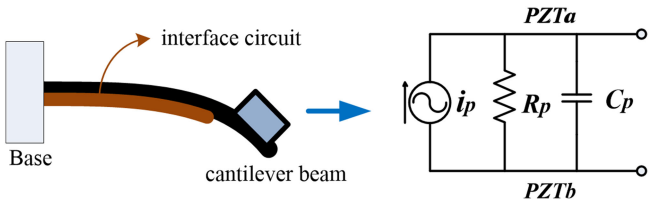

Fig. 1. Cantilever-based PZT harvester and its simplified equivalent circuit.

Vibration EH using piezoelectric transducers (PZTs) have received much attention recently due to high output power and compatibility. Generally, a weakly coupled PZT harvester can be represented by a simplified electrical model as in Fig. 1, which is a parallel circuit consisting of $i_{\rm p}$, $C_{\rm p,}$ and $R_{\rm p}$ [6]. The vibration of the PZT outputs the alternating current (ac) voltage while common miniature electronic devices need a stable direct current (dc) power supply. Therefore, an ac–dc energy extraction interface circuit between the PZT and the electrical equipment is required [7]. The simplest one is the standard energy harvesting (SEH) circuit consisting of only four diodes. However, the harvesting efficiency is low because of the existence of parasitic capacitor in the piezoelectric element (PE) and a phase difference between the voltage and current resulting in reactive power in such a circuit.

The synchronous electric charge extraction (SECE) method is a well-known extraction technique for PZT harvesters. Lefeuvre *et al.* [8] proposed a transformer-based SECE circuit, and achieved a power improvement of 400% compared to the SEH. Some SECE based EH ICs have been developed, such as SECE circuit with residual charge inversion (SECE-RCI) by Dini *et al.* [9], adaptive pulsed synchronous charge extractor circuit by Hehn *et al.* [10] and multishot synchronous electric charge extraction (MS-SECE) by Gasnier *et al.* [11]. But either quiescent current dissipation or precharged power is required to start high-efficiency harvesting circuit properly in these designs. To solve the self-powered and control problems, several interface circuits were proposed on the SECE topology, such as self-powered optimized SECE by Wu *et al.* [12] and self-powered efficient SECE by Shi *et al.* [13]. However, the passive peak detector

Manuscript received August 14, 2020; revised December 4, 2020; accepted January 24, 2021. Date of publication January 27, 2021; date of current version May 5, 2021. This work was supported in part by the National Natural Science Foundation of China under Grant U1709218, Grant 61771268, Grant 61971389, Grant 61801253, and Grant 61601429, in part by the Natural Science Foundation of Zhejiang Province Grant LZ20F010006 and Grant LY20F010003, in part by the Natural Science Foundation of Ningbo Grant 2018A610091, Grant 2019A610113, and in part by the K. C. Wong Magna Fund in Ningbo University. Recommended for publication by Associate Editor B. Semail. *(Corresponding author: Yinshui Xia.)*

Zhidong Chen is with the Faculty of Electrical Engineering and Computer Science, Ningbo University, Ningbo 315211, China, and also with the Zhejiang Business Technology Institute, Ningbo 315012, China (e-mail: 1701082016@nbu.edu.cn).

Yinshui Xia, Xiudeng Wang, Huakang Xia, and Yidie Ye are with the Faculty of Electrical Engineering and Computer Science, Ningbo University, Ningbo 315211, China (e-mail: xiayinshui@nbu.edu.cn; 1611082572@nbu.edu.cn; xiahuakang@nbu.edu.cn; yeyidie@nbu.edu.cn).

Ge Shi is with the College of Mechanical and Electrical Engineering, China Jiliang University, Hangzhou 310018, China (e-mail: shige@cjlu.edu.cn).

Color versions of one or more of the figures in this article are available online at https://doi.org/10.1109/TPEL.2021.3054982.

Digital Object Identifier 10.1109/TPEL.2021.3054982

(PKD) circuit yields a significant phase lag, which seriously reduces the harvesting efficiency.

The synchronized switch harvesting on inductor (SSHI) method is another well-known extraction technique for PZT harvesters. By setting switches and inductor in parallel with the PZT, Guyomar *et al.* [14] proposed a P-SSHI circuit. Lefeuvre *et al.* [15] connected switches and inductor in series with the PZT to form an S-SSHI circuit. Self-powered, improved, and integrated versions of SSHI have then been proposed. Chen *et al.* [16] proposed an improved self-powered P-SSHI (ISP-PSSHI) interface circuit; its peak EH power can reach 3.6 times that of the SEH circuit. Aktakka *et al.* [17] proposed a microinertial EH platform with self-supplied power management circuit, which is intended for autonomous wireless sensor nodes. A variety of research works have demonstrated that a high-quality SSHI circuit can achieve a significant power improvement of 800% compared to the SEH [14], [15]. However, their harvested power is greatly influenced by the capacitor voltage of the rectifier filter and load impedance. The drawback can be addressed by employing maximum power point tracking (MPPT) techniques [18], [19]. Saggini *et al.* [18] proposed an optimal EH solution by means of the resistive and reactive load matching. Costanzo *et al.* [19] proposed an active electronic interface for maximizing the power by means of a multivariable MPPT technique, which can dynamically adjust to ensure that the maximum power. Another SSH implementation is called synchronized switch harvesting on capacitors that uses switched-capacitor instead of bulky inductors and can be fully integrated using the CMOS technology [20], [21].

Numerous EH interface circuits for single PZT have been reported in the literature above. However, one vibration source can share multiple PZTs to harvest more energy. Hence, varieties of multi-input energy harvesters with a single inductor configuration are proposed [22]–[25]. Romani *et al.* [22] proposed a fully autonomous EH circuit for arrays of PZTs based on SECE technique. Shareef *et al.* [23] employed a rectifierless ac–dc interface circuit for low-voltage PZTs to improve the conversion efficiency at low input voltages. Meng *et al.* [24] proposed a PEH chip for harvesting piezoelectric energy from multi-PZTs with a shared inductor. These circuits harvest piezoelectric energy from multiple PZTs to share a single inductor with time-division multiplexing [22]–[24]. In practice, the phase of different PZTs installed on the same vibration source may be synchronized. Hence, it is necessary that the PZTs use the single inductor at the same time. Wang *et al.* [25] proposed an extensible multi-input piezoelectric EH circuit for multiple PZTs, and solve the problems of mutual influence of multiple PZTs under the same phase.

However, these multiple piezoelectric EH circuits are based on the SECE, which can maintain high output power only under low-coupled or off-resonance PZTs [26], [27]. In addition, the efficiency of the SECE is low when the output voltage is low, because part of the energy extracted from the PZT is consumed by the freewheeling diode [23].

In view of the above problems, this article expands typical S-SSHI into a multi-input topology interface and a self-powered multi-input serial synchronized switch harvesting on inductor

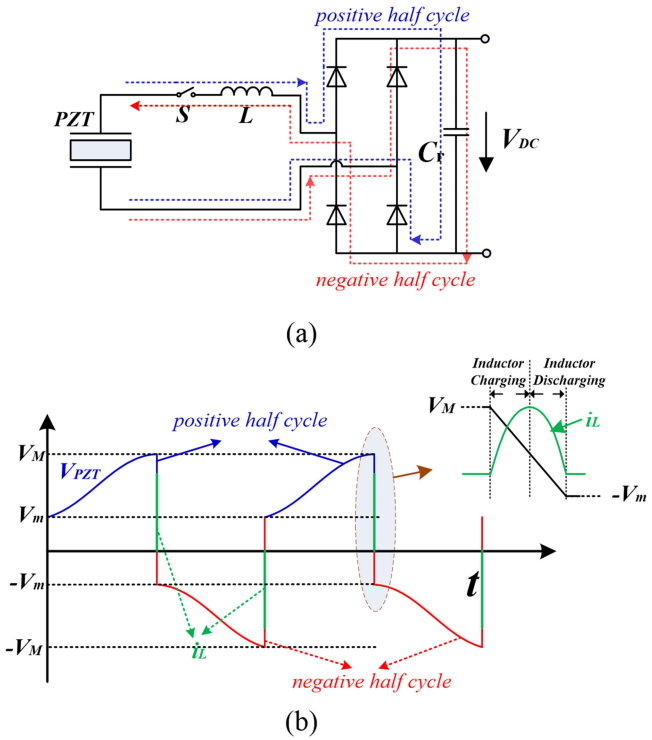

Fig. 2. Circuit and waveforms of the S-SSHI. (a) Typical S-SSHI circuit. (b) Waveforms of the typical S-SSHI circuit.

(MIS-SSHI) circuit was proposed and implemented. Besides, the diodes in traditional S-SSHI circuit are removed to improve the conversion efficiency. The proposed MIS-SSHI circuit can harvest energy from multiple PZTs available for arbitrary phase difference (0-2π) with a single inductor and its input ports are expandable according to the needs of the application scenario.

In Section II, the working principle of the typical S-SSHI and proposed MIS-SSHI are introduced. In Section III, the implementation of a self-powered MIS-SSHI circuit is described. In Section IV, the experimental work is provided. Finally, the conclusion is drawn in Section V.

II. Proposed MIS-SSHI Topology

A. Analysis of the Typical S-SSHI

As shown in Fig. 2(a), the traditional S-SSHI interface circuit is composed of a nonlinear processing circuit connected in parallel with the PZT and the input of the rectifier bridge. The nonlinear processing circuit is only composed of an inductor L in series with a switch S.

During most of the time in one cycle, the PZT is in open-circuit configuration. When the voltage of the PZT V_{PZT} reaches the peak, that is, the energy accumulated on C_{p} reaches the maximum V_{M}, the switch S is turned ON immediately. When the switch S is turned ON, the inductor L and the capacitor C_{p} form an LC resonance loop. After 1/4 resonance period T, the current of the inductor L reaches a peak, while the energy accumulated on C_{p} is transferred to the inductor L and the output capacitor C_{r}. This can be called inductor charging stage and the resonance

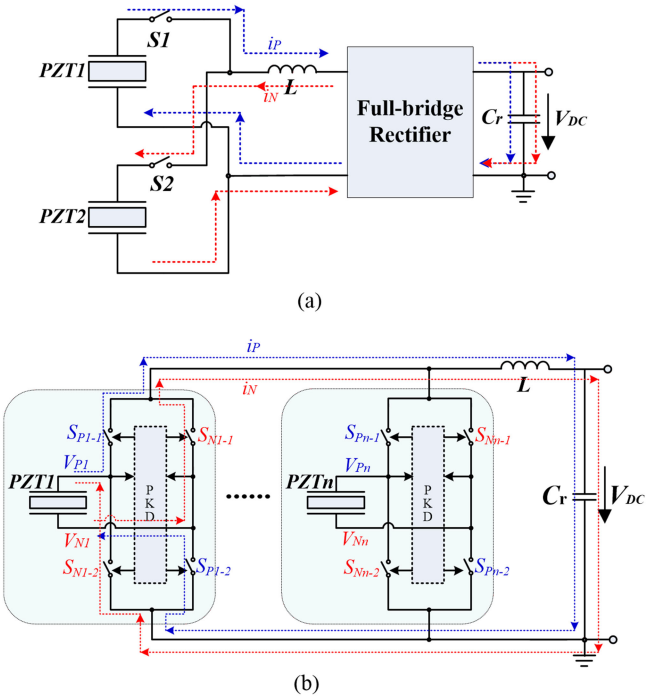

Fig. 3. Multi-input EH circuits based on S-SSHI technique. (a) Typical S-SSHI topology. (b) Proposed MIS-SSHI topology.

period T can be expressed as

$$T = 2\pi\sqrt{LC_{\mathrm{p}}}. \tag{1}$$

After another 1/4 resonance period T, the current of the inductor drops to 0, while the energy accumulated on L is transferred to C_{p} and C_{r}. This can be called inductor discharging stage. At those instants, the voltage on C_{p} inversions from V_{M} to $-V_{\mathrm{m}}$ occurs. The voltages on C_{p} and current on L are drawn in Fig. 2(b).

B. Proposed MIS-SSHI Topology

It can be seen that the inductor current in typical S-SSHI circuit is opposite in positive and negative half cycle as shown in Fig. 2. Therefore, it is difficult for the typical S-SSHI to be directly expanded into a multi-input topology interface. The main issue is that the mutual influence of multiple PZTs under some special phase differences. For example, the phase difference between two PZTs is exactly π. And both PZTs begin to transfer energy to the single inductor at the same time as shown in Fig. 3(a). The PZT1 works in the positive half cycle while the PZT2 does in the negative half cycle. When switches *S1* and *S2* are turned ON at the same time, the PZT1 charges the inductor in one direction while the PZT2 charges the inductor in the other direction at the same time, and the energy in the inductor will be consumed.

The proposed S-SSHI topology allows the inductor to maintain a unidirectional current in both positive and negative half cycles, as shown in Fig. 3(b), which is convenient to be extended to a multi-input interface circuit. It is composed of an inductor

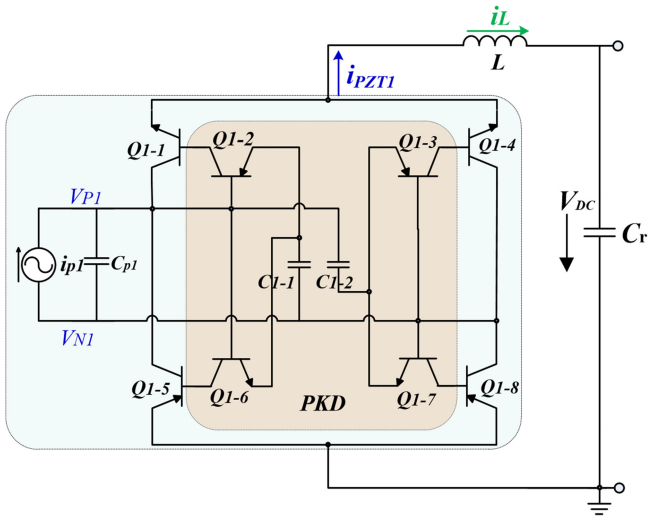

Fig. 4. MIS-SSHI circuit with single PZT cell.

L, a storage capacitor C_{r} and multiple PZT cells. The PZT cell includes a PZT, four switches, and a PKD.

During the positive half cycle, when the open-circuit voltage of the PZTn (n≥1) reaches the peak, the PKD turn ONthe switches $S_{\mathrm{Pn\text{-}1}}$ and $S_{\mathrm{Pn\text{-}2}}$, so that the capacitor C_{r}, the inductor L, and the parasitic capacitor of PZTn form an LC resonance loop. After the 1/2 resonance period T, the voltage inversion from V_{M} to $-V_{\mathrm{m}}$ occurs as Fig. 2(b), and the energy is transferred to the output capacitor C_{r}. During the negative half-cycle, the PKD turn ON the switches $S_{\mathrm{Nn\text{-}1}}$ and $S_{\mathrm{Nn\text{-}2}}$, and the proposed circuit works in a similar way. Based on this way, it can be guaranteed that the inductor current has the same direction in the positive and negative half cycles as shown in Fig. 3(b). And the diodes in the typical S-SSHI circuit are replaced by four switches to reduce energy loss. Then, multi-input S-SSHI piezoelectric energy harvester is achieved.

III. Implementation of the MIS-SSHI

To explain the working principle of the circuit clearly, two specific implementations of the MIS-SSHI circuit are used to introduce the extraction for single PZT and the extractions for multiple PZTs, respectively.

A. Extraction for Single PZT

Fig. 4 shows the self-powered MIS-SSHI circuit for single PZT cell. V_{P1} and V_{N1} represent two output pins of the PZT1. The capacitors $C_{1\text{-}1}$, $C_{1\text{-}2}$ and bipolar transistors $Q_{1\text{-}2}$, $Q_{1\text{-}3}$, $Q_{1\text{-}6}$, $Q_{1\text{-}7}$ constitute the PKD, which acts to turn ON the switches ($Q_{1\text{-}1}$, $Q_{1\text{-}4}$, $Q_{1\text{-}5}$ and $Q_{1\text{-}8}$). When the open-circuit voltage of the PZT1 reaches a peak, the energy generated from PZT1 can be transferred to the output capacitor C_{r}. To explain its working principle, the four stages called natural charging, current reversing, inductor charging, and inductor discharging are analyzed as follows.

1) *Natural Charging Stage (t_0~t_1):* in the period of positive half-cycle, $V(V_{\mathrm{P1}}) > V(V_{\mathrm{N1}})$, i_{p} charges the capacitors

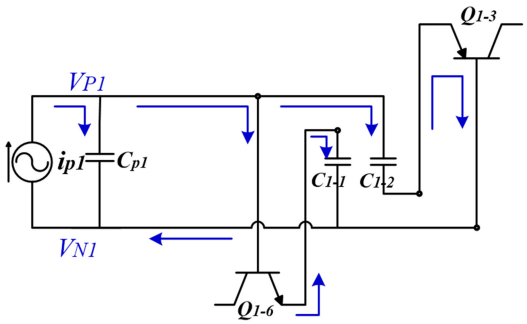

Fig. 5. Working stages of natural charging stage.

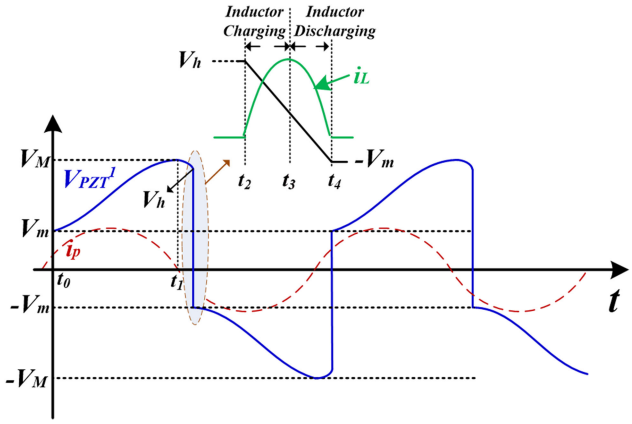

Fig. 6. Waveforms of the proposed circuit for single PZT.

C_{p1} of the PZT1 as shown in Fig. 5, also charges the capacitors $C_{1\text{-}1}$ and $C_{1\text{-}2}$ gradually through $Q_{1\text{-}6}$ base-emitter junction and $Q_{1\text{-}3}$ emitter-base junction, respectively.

At t_1 instant, the voltage V_{PZT1} on C_p reaches a maximum value V_M as shown in Fig. 6. The peak voltage V_M is given by

$$V_M = V_m + 2\frac{\alpha u_M}{C_{p1} + 2C_{1-1} + C_{1-2}} \tag{2}$$

where V_m is the inversion voltage of the previous half cycle, α and u_M are the piezoelectric force-voltage factor, and the peak displacement of the PZT, respectively.

2 *Current Reversing Stage (t_1~t_2):* in this stage, the PZT1 voltage V_{PZT1} begins to decrease because the PZT changes its direction. The V_{PZT1} decreases gradually as shown in Fig. 6 while the voltages of $C_{1\text{-}1}$ and $C_{1\text{-}2}$ voltage keep constant because emitter-base junction of $Q_{1\text{-}6}$ and $Q_{1\text{-}7}$. At t_2 instant, when V_{PZT1} decreases below V_h, it means the current reversing stage is ended. The EH voltage V_h can be expressed as

$$V_h = V_M - 2V_{BE} \tag{3}$$

where V_{BE} is the threshold voltage of the corresponding transistors.

3) *Inductor Charging Stage (t_2~t_3):* At t_2 instant, the $C_{1\text{-}1}$ voltage is applied to $Q_{1\text{-}1}$ base through $Q_{1\text{-}2}$ emitter–collector while the $C_{1\text{-}2}$ voltage is applied to $Q_{1\text{-}8}$ base through $Q_{1\text{-}7}$ collector–emitter as shown in Fig. 7, so that

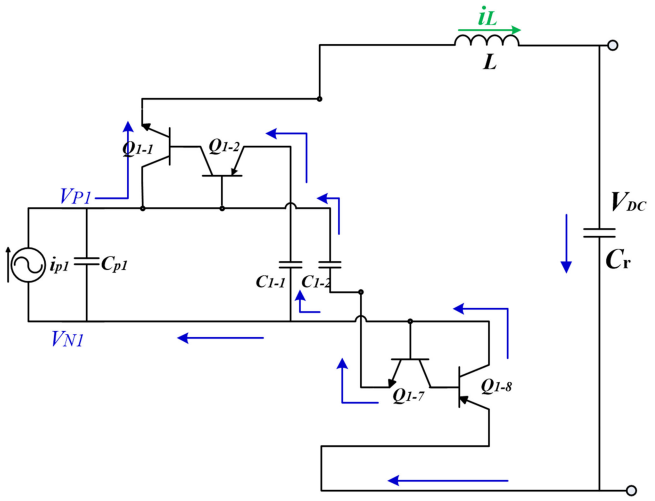

Fig. 7. Working stages of inductor charging stage.

$Q_{1\text{-}1}$ and $Q_{1\text{-}8}$ switch ON immediately. As a result, the LC oscillation among the capacitor C_{p1}, $Q_{1\text{-}1}$ collector–emitter, L and C_r and $Q_{1\text{-}8}$ emitter–collector is established. The energy on C_{p1} begins to transfer to inductor L and the output capacitor C_r. In addition, the energy on capacitor $C_{1\text{-}1}$ is transferred to L and C_r with a loop of $C_{1\text{-}1}$, $Q_{1\text{-}2}$ (EC), $Q_{1\text{-}1}$ (BE), L, C_r and $Q_{1\text{-}8}$ (EC). So, does the energy on capacitor $C_{1\text{-}2}$.

The inductor charging stage starts only when V_h is larger than the voltage drop produced by $Q_{1\text{-}1}$ (CE), $Q_{1\text{-}8}$ (EC), and C_r in series. Yield the constraint for V_h as

$$V_h > 2V_{CE(sat)} + V_{DC} \tag{4}$$

where $V_{CE(sat)}$ is the collector–emitter saturation voltage of the corresponding transistors. On the other hand, from (3) and (4), we can obtain the maximum attainable V_{DC} in EH from (4) as follows:

$$V_{DC,max} = V_M - 2V_{CE(sat)} - 2V_{BE}. \tag{5}$$

At this stage, the harvesting process starts, C_p charges the inductor L and capacitor C_r, which causes a decrease in V_{PZT1} and an increase in the inductor current i_L is as shown in Fig. 6. After the first 1/4 LC oscillation, the inductor current i_L increases to its peak, which means the inductor charging stage is over.

4) *Inductor Discharging Stage (t_3~t_4):* At t_3 instant, the inductor current i_L increases to its peak. After another 1/4 resonance period, the current of the inductor drops to 0, while the energy accumulated on L is transferred to C_p and C_r. The inductor discharging stage is over. Fig. 6 shows the voltages V_M and the inversion voltage V_m before and after the inversion process, the relation between V_h and V_m can be expressed as

$$\begin{aligned} &-V_m - V_{DC} - 2V_{CE(sat)} \\ &= -(V_h - V_{DC} - 2V_{CE(sat)})e^{-\pi/2Q_i} \end{aligned} \tag{6}$$

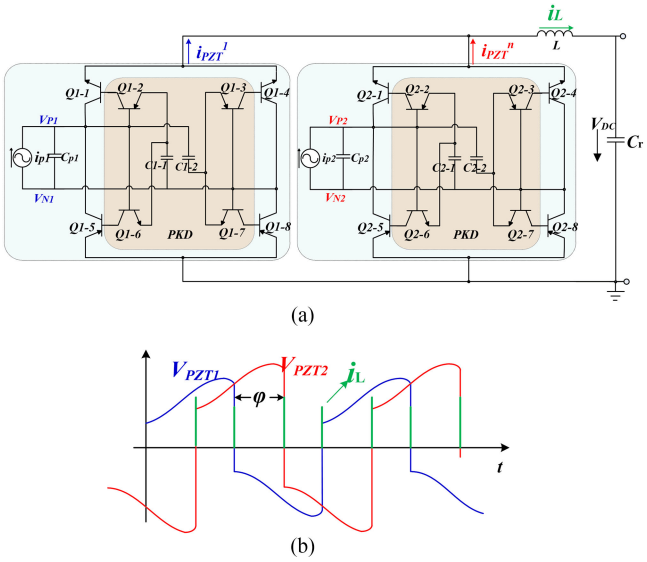

Fig. 8. Circuit and waveforms with two PZT cells. (a) Circuit. (b) Waveforms.

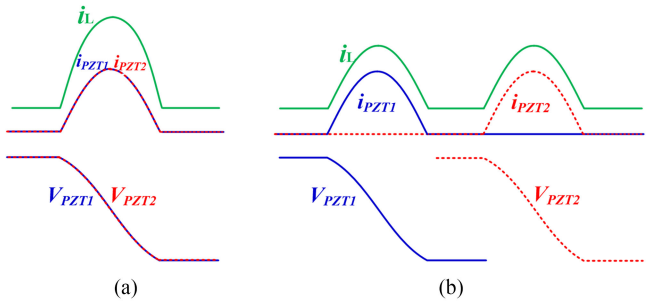

Fig. 9. Voltage and current waveforms of (a) synchronization, (b) asynchronization.

where $Q_{\rm i}$ is the electrical quality factor and can be defined as

$$Q_{\rm i} = \frac{1}{r}\sqrt{\frac{L}{C_{\rm p1} + C_{1-1} + C_{1-2}}} \tag{7}$$

where r is the internal resistor of L. Based on the above analyses, the harvested power during the harvesting process in the proposed circuit for single PZT can be calculated as follows:

$$P_{\rm h} = 2f \cdot V_{\rm DC} \cdot \int_{t_2}^{t_3} i_L(t){\rm d}t = 2f \cdot V_{\rm DC} \cdot \int_{t_2}^{t_2+T/2} i_L(t){\rm d}t$$
$$= 2f \cdot V_{DC}(C_{\rm p1} + C_{1-1} + C_{1-2}) \cdot (V_{\rm h} + V_{\rm m}). \tag{8}$$

The dissipated power during the harvesting process can be calculated as follows:

$$P_{\rm d} = f\{(C_{\rm p1} + C_{1-1} + C_{1-2})\,[(V_h - V_{DC} - 2V_{CE(sat)})^2$$
$$- (-V_m - V_{DC} - 2V_{CE(sat)})^2]$$
$$+ 4V_{CE(sat)}[(C_{\rm p1} + C_{1-1} + C_{1-2})(V_{\rm h} + V_{\rm m})\,]\} \tag{9}$$

where f is the vibration frequency. Two items in (9) estimate the power dissipations produced by the nonideal voltage inversions and voltage drops of the components.

B. Extractions for Multiple PZTs

In the actual environment, the vibration amplitude and frequency of the PZTs vary from time to time, which causes the phase differences between the PZTs uncertain. When the phase difference φ is very small, the PZTs may occupy the inductor at the same time. Generally, inductor controlling technique is needed to ensure the different inductor access time of the PZTs.

The proposed MIS-SSHI circuit can handle inductor access conflict when multiple PZTs charge the inductor simultaneously, without using extra inductor controlling circuit. Fig. 8(a) shows the self-powered MIS-SSHI circuit for multiple PZT cells. It contains two PZT cells to explain how the two sources of ac energy are extracted with a single inductor with arbitrary phase difference ($0-2\pi$). When two PZTs are connected to the proposed circuit, the waveforms of the PZTs are shown in Fig. 8(b), in which φ is the phase differences between two PZTs, $V_{\rm PZT1}$ and $V_{\rm PZT2}$ are voltage across PZT1 and PZT2.

There are countless possibilities for the phase difference φ between the PZTs and it is difficult to analyze them one by one. For a clearer analysis, the phase difference φ between the two PZTs is divided into four cases as follows. $i_{\rm L}$ is the current on the inductor L. $i_{\rm PZT1}$ and $i_{\rm PZT2}$ are the current through PZT1 cell and PZT2 cell, respectively.

1) *Synchronization:* The inductor access time of PZT1 and PZT2 are at the same. In this case, the phase difference φ is equal 0. BJTs $Q_{1\text{-}1}$, $Q_{1\text{-}8}$, $Q_{2\text{-}1}$, and $Q_{2\text{-}8}$ are turned ON simultaneously. PZT1 cell and PZT2 cell are connected in parallel, which form an LC loop in series with L and $C_{\rm r}$. The waveforms of PZT1 and PZT2 are overlap and the inductor current $i_{\rm L}$ is the sum of the currents of PZT1 cell and PZT2 cell as shown in Fig. 9(a).
2) *Asynchronization:* According to the previous description of the working principle of the S-SSHI, the inductor operating time is very short compared with the vibration period. Therefore, in this case, two PZT cells work independently, and the inductor access times of two PZTs are separated as shown in Fig. 9(b). In most cases, two PZTs work at this state and they do not affect each other.
3) *Uncompleted Inductor Charging:* In this case, the voltage $V_{\rm PZT1}$ of the PZT1 first reaches its EH voltage and BJTs $Q_{1\text{-}1}$, $Q_{1\text{-}8}$ are turned ON. The PZT1 begins to charge the inductor L while $V_{\rm PZT1}$ begins to decrease at time t_0 as shown in Fig. 10(a). At time t_1, the inductor charging stage of PZT1 is not completed, the voltage $V_{\rm PZT2}$ of the PZT2 reaches its EH voltage and BJTs $Q_{2\text{-}1}$, $Q_{2\text{-}8}$ are turned ON. The PZT2 begins to charge the inductor L and $V_{\rm PZT2}$ begins to decrease as shown in Fig. 10(a). Because $V_{\rm PZT2} > V_{\rm PZT1}$, BJTs $Q_{1\text{-}1}$, $Q_{1\text{-}8}$ are temporarily turned OFF while $V_{\rm PZT1}$ remains unchanged. The charge in the PZT2 is preferentially extracted. At the time t_2, the voltages of the PZT1 and PZT2 are equal ($V_{\rm PZT1} = V_{\rm PZT2}$), BJTs $Q_{1\text{-}1}$, $Q_{1\text{-}8}$, $Q_{2\text{-}1}$, $Q_{2\text{-}8}$ are turned ON, both PZT1 and PZT2 charge the inductor simultaneously. After the inductor current reaches the peak (the inductor

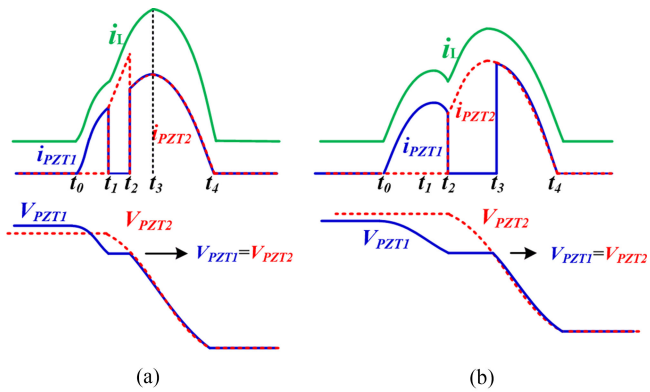

Fig. 10. Voltage and current waveforms of: (a) uncompleted inductor charging; (b) Completed inductor charging.

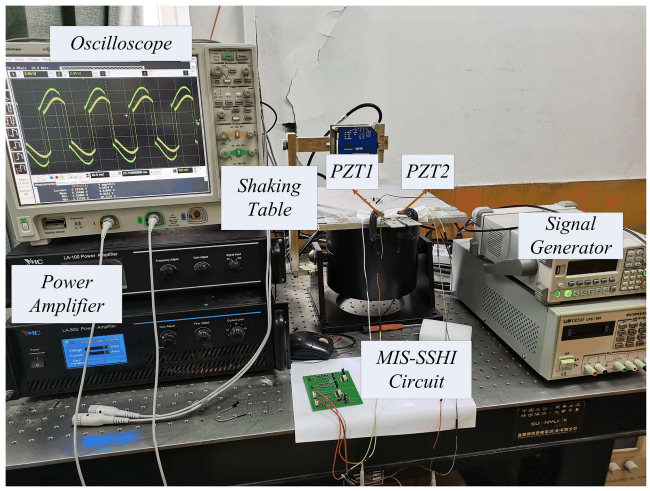

Fig. 11. Experimental setup.

charging stage is over), the circuit begins to enter the inductor discharging phase.

4) *Completed Inductor Charging:* In this case, when the PZT1 is at the inductor discharging stage while the energy in the inductor has not been completely released as shown in Fig. 10(b). The voltage V_{PZT2} of the PZT2 reaches its EH voltage and BJTs $Q_{2\text{-}1}$, $Q_{2\text{-}8}$ are turned ON. At this time, V_{PZT2} is larger than V_{PZT1}, hence the charge in the PZT2 is preferentially extracted. At the time t_3, the voltages of the PZT1 and PZT2 are equal ($V_{\mathrm{PZT1}} = V_{\mathrm{PZT2}}$). BJTs $Q_{1\text{-}1}$, $Q_{1\text{-}8}$, $Q_{2\text{-}1}$, $Q_{2\text{-}8}$ are turned ON, both PZT1 and PZT2 charge the inductor simultaneously. Then, the currents from the two become the same until the inductor discharging stage is completed.

According to the analysis of the above four cases, it can be found that the MIS-SSHI circuit proposed in this article can harvest PE from multiple PZTs at arbitrary phase difference.

IV. Experimental Work

In order to verify the effectiveness of the proposed MIS-SSHI circuit, the experimental platform is built as shown in Fig. 11.

TABLE I
Components

Component	Models Or Values
PZT	PPA-1014
Q_1, Q_4, Q_6, Q_7	2N3904
Q_2, Q_3, Q_5, Q_8	2N3906
C_1, C_2	5.6nF
C_r	10uF
L	2.3mH(2.1Ω)

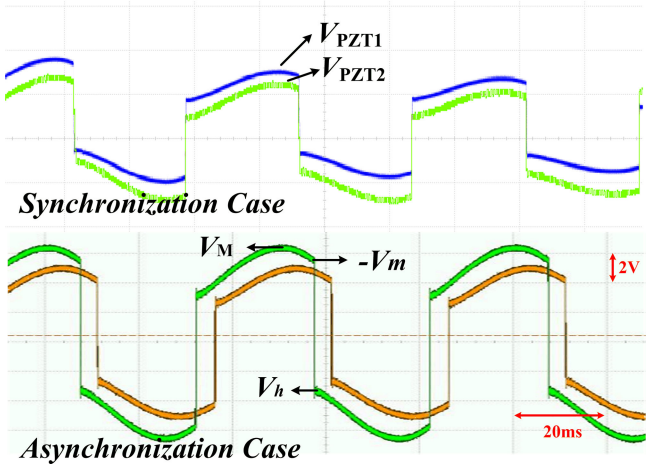

Fig. 12. Experimental waveforms.

The experimental system consists of a function signal generator, an oscilloscope, two PZTs, a power amplifier, a shaking table, and the MIS-SSHI EH interface circuit. One end of the PZTs is tightly fixed with a metal mass, and the other end is fixed on the shaking table. Two commercial cantilever-based PZT harvesters, PPA-1014 ($C_{\mathrm{p}} = 41$ nF) from Mide Technology, were employed in the measurement. The vibration frequency and amplitude of the vibrating table was adjusted by the signal generator and power amplifier. The proposed circuit was fabricated using the discrete components as listed in Table I.

Both PZTs are attached on the same vibrating table. The resonant frequencies of the PZTs can be adjusted by the weight and position of the mass. Then, the signal generator and power amplifier are adjusted to make the vibrating table working at different frequency and amplitude, and the phase difference between the PZTs is changed. Fig. 12 shows the voltage waveforms measured by the oscilloscope, which corresponds to the output voltage of the PZTs with synchronization and asynchronization cases.

The voltage difference between the maximum voltage V_{M} and the EH voltage V_{h} is about 1.2 V. It is mainly caused by V_{BE} as shown in (3). Within the semiperiod of vibration *T*/2 (inductor charging and inductor discharging stages), the voltage V_{PZT1} of the PZT drops from V_{h} to $-V_{\mathrm{m}}$. The relation between V_{h} and V_{m} is shown in (8). The dissipated power during the harvesting process is shown in (9).

Fig. 13 shows the measured inductor current and output voltage waveforms in the experiment, in which there is an enlarged view about inductor current called inductor charging stage and inductor discharging stage. It can be seen that the inductor

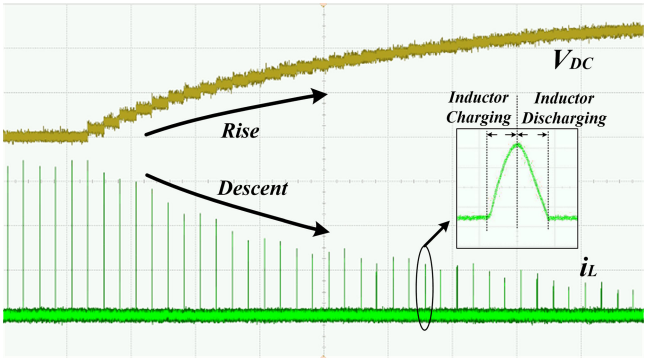

Fig. 13. Inductor current and output voltage waveform.

currents in the positive and negative half cycles are at the same direction.

The output voltage $V_{\rm DC}$ rises instantaneously corresponding to each inductor current pulse, which is similar to a staircase. However, the inductor current $i_{\rm L}$ decreases with the increase of the output voltage $V_{\rm DC}$. The reason is that the output voltage $V_{\rm DC}$ limits the inductor current $i_{\rm L}$. Without considering the *LC* resonant loss, the peak current can be simplified as

$$i_{L,\max} = \sqrt{\frac{C_p}{L}} \cdot (V_M - 2V_{BE} - 2V_{CE(sat)} - V_{DC}). \quad (10)$$

The output voltage $V_{\rm DC}$ increases gradually until the inductor current drops to 0. That means the proposed circuit cannot harvest energy from the PZT. The maximum attainable $V_{\rm DC}$ in EH is shown in (5). That is why the S-SSHI based circuit can only maintain high efficiency only under the optimal output voltage.

To verify whether the MIS-SSHI circuit can handle inductor access conflict, we used two identical PZTs (PPA-1014). Both PZTs are attached on the same vibrating table. The resonant frequencies of the PZTs can be adjusted by the weight and position of the mass. Then, the signal generator and power amplifier are adjusted to make the vibrating table working at different frequency and amplitude, and the phase difference between the PZTs is changed. Then, we tested the voltage waveforms of the PZTs and current waveforms of the inductor at the instant when the inductor needs to be accessed by both PZTs, as shown in Fig. 14. The phase difference between the two PZTs is divided into four cases as analyzed in "*Extractions for multiple PZTs*" section.

Fig. 14(a) shows the inductor current with the synchronization case. The phase differences of the two PZTs are exactly 0. The waveforms of PZT1 and PZT2 are overlapped and the inductor current $i_{\rm L}$ are the sum of the currents of PZT1 cell and PZT2 cell as shown in Fig. 14(a). Fig. 14(b) shows the inductor current with the asynchronization case in which two PZTs share the inductor with time-division multiplexing, the inductor access time of two PZTs are separated. Fig. 14(c) shows the inductor current with the uncompleted inductor charging case in which the PZT1 enters the inductor charging stage and is uncompleted when the PZT2 begins to charge the inductor. It can be seen that $V_{\rm PZT1}$ remains unchanged until the voltages of the PZT1

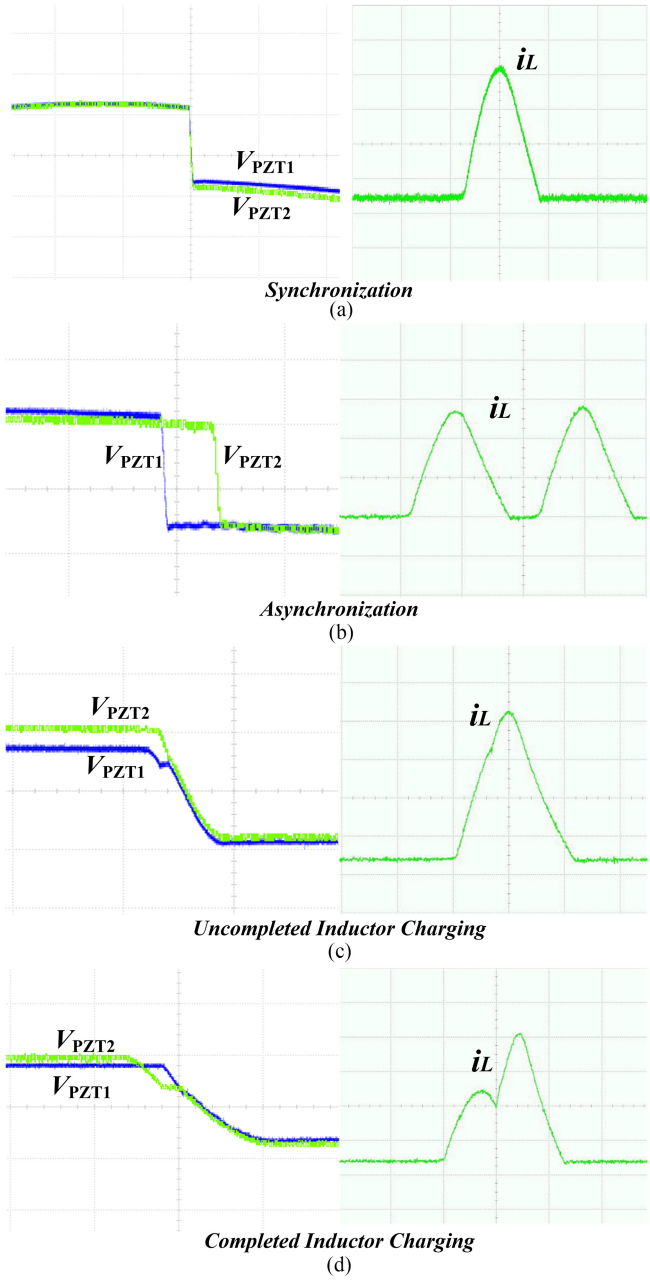

Fig. 14. Voltage waveforms of two PZTs and inductor current waveforms in four cases. (a) Synchronization. (b) Asynchronization. (c) Uncompleted inductor charging. (d) Completed inductor charging.

and PZT2 are equal ($V_{\rm PZT1} = V_{\rm PZT2}$). Fig. 14(d) shows the inductor current with the completed inductor charging case. The PZT2 enters the inductor discharging stage and is uncompleted when the second PZT begins to charge the inductor. $V_{\rm PZT2}$ remains unchanged until the voltages of the PZT1 and PZT2 are equal ($V_{\rm PZT1} = V_{\rm PZT2}$). Theoretical analysis and experimental results show that the proposed circuit can handle inductor access conflict when multiple PZTs charge the inductor simultaneously, without using extra inductor controlling circuit.

To measure the harvested power of the MIS-SSHI circuit for single PZT, the signal generator is adjusted to make the PZT1

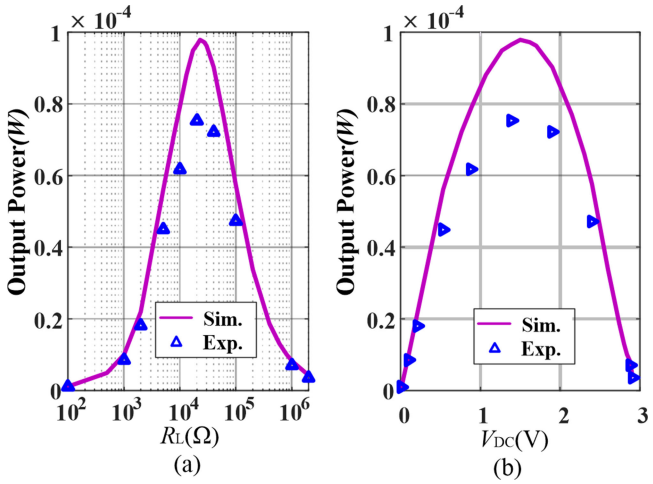

Fig. 15. Measured and simulated output power of the MIS-SSHI for single PZT ($V_{oc} = 6$V, $f = 19$ Hz). (a) Output power versus load resistance R_L. (b) Output power versus the output voltage V_{DC}.

working near its resonance frequency 19 Hz and the open-circuit voltage of PZT1, $V_{OC1} = 6$ V. Then, the PZT1 is connected to the proposed circuit. The measured output power of the MIS-SSHI circuit with its simulated and experimental results are compared for single PZT under different R_L and V_{DC} when the open-circuit voltages $V_{oc} = 6$ V in Fig. 15. It can be seen that their power curves are similar in terms of trend and shape. However, the measured results are smaller than those in the simulation. The maximum deviation is about 20%. This is that the simulations adopt the simplified equivalent circuit, which does not consider the mechanical effects induced by power extraction leading to the overestimation of its performance.

In order to measure the harvested power of the MIS-SSHI circuit for multiple PZTs, two PZTs are connected to the proposed circuit. The resonance frequencies of PZT1 and PZT2 are about 18.7 and 19.2 Hz, respectively. The signal generator is adjusted to make the PZT1 and PZT2 working near their resonance frequency 19 Hz. The open-circuit voltage of PZT1 and PZT2 are measured ($V_{oc1} = 5.8$ V, $V_{oc2} = 5.2$ V).

The test experiment results are shown in Fig. 16 and the output power of the SEH circuit for single PZT and two PZTs are used as a reference under the same open-circuit voltage.

The maximum output power of the MIS-SSHI for single PZT can reach 3.7 times of that of the SEH circuit. From Fig. 16(a), it can be seen that the output power of the MIS-SSHI circuit is affected by the load resistance R_L. And for single PZT EH, the optimum load resistance R_L is about 18k while for two PZTs EH, the optimum load resistance R_L is about 12k. It can be concluded that the optimum load resistance and the power curves are offset to the left. This is because the output voltage V_{DC} will rise under the same load resistance for the EH of two PZTs, and reduce the output power. In Fig. 16(b), it can be seen that the output power reduces when the output voltage V_{DC} exceeds the optimum output voltage. There are different optimum output voltages for PZT1 and PZT2 because of their different open-circuit voltage. The optimum output voltage of PZT1 and PZT2 are about 1.45 and 1.3 V, respectively.

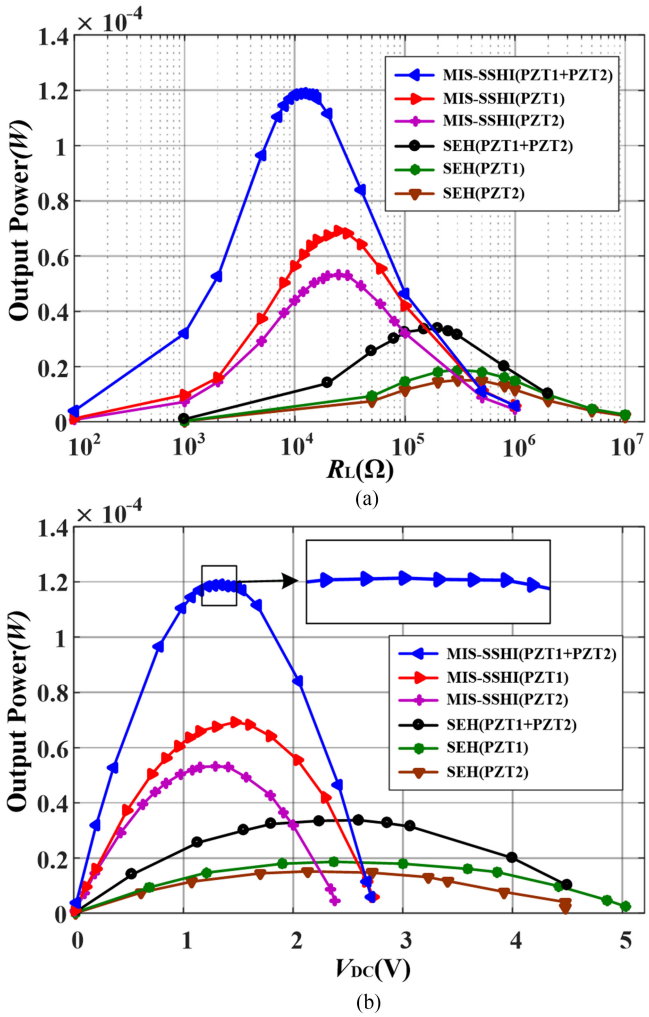

Fig. 16. Measured output power of the MIS-SSHI for two PZTs ($V_{oc1} = 5.8$ V, $V_{oc2} = 5.2$ V, $f = 19$ Hz). (a) Output power versus load resistance RL. (b) Output power versus the output voltage VDC.

When the proposed circuit harvests energy from both PZT1 and PZT2, the optimum output voltage is between 1.45 and 1.3 V. The output power almost remains unchanged in this output voltage range, in which there is an enlarged view about the output power in Fig. 16(b). This is because when the output voltage V_{DC} exceeds the optimum output voltage of PZT2 (1.3 V), the output power of PZT2 decreases while the output power of PZT1 increases with the increase of V_{DC}, and the hybrid output power of PZT1 and PZT2 is almost unchanged. It can be seen that the harvest power from the dual PZTs is significantly higher than that from the single PZT, and the integration efficiency for dual PZTs can reach 98%. This means that the MIS-SSHI circuit is capable of extracting energy from multiple PZTs based on S-SSHI technique. And its input ports are expandable according to the needs of the application scenario.

Table II provides a performance comparison with the state-of-the-art PZT EH circuits. The circuits proposed in [3] and [16] are the S-SSHI based and P-SSHI based EH circuits for single PZT, respectively. The circuits proposed in [22], [23], and [25]

TABLE II
PERFORMANCE COMPARISON

Publication	TIE2012[3]	TPEL2019 [16]	TPEL2014[22]	TPEL2019[23]	TIE2020[25]	This work
PZT	N/A	N/A	Q220-A4-303YB	PPA4011	PPA1014	PPA1014
Technique	S-SSHI	P-SSHI	SECE	SECE	SECE	S-SSHI
Multi-input	NO	NO	YES	YES	YES	YES
Inductor	47mH	50mH	10mH	3.3mH	1mH	2.3mH
Self-powered	YES	YES	NO	NO	YES	YES
Synchronous extraction for multiple PZTs	N/A	N/A	NO	NO	YES	YES
Boost to SEH(max)	3×	3.6×	N/A	N/A	3×	3.7×
Frequency	30Hz	50Hz	40Hz	65Hz	18.6Hz	19Hz

demonstrated three implementations of SECE circuit, capable of handling multiple PZTs.

Compared with the single PZT EH circuits [3] and [16], the proposed circuit is of the obvious advantages to harvest more energy. That is because the diodes in these circuits cause energy loss, which seriously reduces the harvesting efficiency. In [22] and [23], discrete implementations based on SECE circuit were demonstrated, which are capable of handling multiple PZTs. In order to produce accurate control signal, a MCU operating under a 200 μA active mode and a comparator with about 500 μA were used, respectively. Hence, there is quiescent current dissipation in these designs which limits their practical applications in WSNs. In [25], a self-powered multi-input circuit for piezoelectric and thermoelectric EH is proposed and it can simultaneously extract energy from multiple PZTs. However, the peak output power can only reach three times of that of the SEH circuit, which is lower than the proposed circuit.

V. CONCLUSION

In this article, the method to simultaneously harvest the energy from multiple PZTs based on S-SSHI technique is presented. A self-powered multi-input serial synchronized switch harvesting on nductor (MIS-SSHI) interface circuit for piezoelectric EH is proposed. The diodes in traditional S-SSHI circuit are removed to improve the conversion efficiency. Both theoretical analysis and experimental test results demonstrate the effectiveness of the MIS-SSHI circuit. The results show that the MIS-SSHI circuit can extract energy from PZTs with arbitrary phase difference.

REFERENCES

[1] S. Chen, H. Xu, D. Liu, B. Hu, and H. Wang, "A vision of iot: Applications, challenges, and opportunities with china perspective," *IEEE Internet Things J.*, vol. 1, no. 4, pp. 349–359, Aug. 2014.

[2] J. A. Stankovic, "Research directions for the internet of things," *IEEE Internet Things J.*, vol. 1, no. 1, pp. 3–9, Feb. 2014.

[3] J. Liang and W. Liao, "Improved design and analysis of self-powered synchronized switch interface circuit for piezoelectric energy harvesting systems," *IEEE Trans. Ind. Electron.*, vol. 59, no. 4, pp. 1950–1960, Apr. 2012.

[4] S. Sudevalayam and P. Kulkarni, "Energy harvesting sensor nodes: Survey and implications," *IEEE Commun. Surv. Tut.,* vol. 13, no. 3, pp. 443–461, Jul./Sep. 2011.

[5] O. B. Akan, O. Cetinkaya, C. Koca, and M. Ozger, "Internet of hybrid energy harvesting things," *IEEE Internet Things J.*, vol. 5, no. 2, pp. 736–746, Apr. 2018.

[6] Y. C. Shu, I. C. Lien, and W. Wu, "An improved analysis of the SSHI interface in piezoelectric energy harvesting," *Smart Mater. Struct.*, vol. 16, no. 6, pp. 2253–2264, 2007.

[7] G. D. Szarka, B. H. Stark, and S. G. Burrow, "Review of power conditioning for kinetic energy harvesting systems," *IEEE Trans. Power Electron.*, vol. 27, no. 2, pp. 803–815, Feb. 2012.

[8] E. Lefeuvre, A. Badel, C. Richard, and D. Guyomar, "Piezoelectric energy harvesting device optimization by synchronous electric charge extraction," *J. Intell. Mater. Syst. Struct.*, vol. 16, no. 10, pp. 865–876, 2005.

[9] M. Dini, A. Romani, M. Filippi, and M. Tartagni, "A nanopower synchronous charge extractor IC for low-voltage piezoelectric energy harvesting with residual charge inversion," *IEEE Trans. Power Electron.*, vol. 31, no. 2, pp. 1263–1274, Feb. 2016.

[10] T. Hehn *et al.*, "A fully autonomous integrated interface circuit for piezoelectric farvesters," *IEEE J. Solid-State Circuits*, vol. 47, no. 9, pp. 2185–2198, Sep. 2012.

[11] P. Gasnier *et al.*, "An autonomous piezoelectric energy harvesting IC based on a synchronous multi-shot technique," *IEEE J. Solid-State Circuits*, vol. 49, no. 7, pp. 1561–1570, Jul. 2014.

[12] Y. P. Wu, A. Badel, F. Formosa, W. Q. Liu, and A. Agbossou, "Self-powered optimized synchronous wlectric charge extraction circuit for piezoelectric energy harvesting," *J. Intell. Mater. Syst. Struct.*, vol. 25, pp. 2165–2176, Nov. 2014.

[13] G. Shi, Y. Xia, Y. Ye, L. Qian, and Q. Li, "An efficient Self-powered synchronous electric charge extraction interface circuit for piezoelectric energy harvesting systems," *J. Intell. Mater. Syst. Struct.*, vol. 27, pp. 2160–2178, Jan. 2016.

[14] D. Guyomar, A. Badel, E. Lefeuvre, and C. Richard, "Toward energy harvesting using active materials and conversion improvement by nonlinear processing," *IEEE Trans. Ultrasonics, Ferroelect. Freq. Control*, vol. 52, no. 4, pp. 584–595, Apr. 2005.

[15] E. Lefeuvre, A. Badel, C. Richard, L. Petit, and D. Guyomar, "A comparison between several vibration-powered piezoelectric generators for standalone systems," *Sensors Actuators A: Phys.*, vol. 126, no. 2, pp. 405–416, 2006.

[16] Z. Chen, J. He, J. Liu, and Y. Xiong, "Switching delay in self-powered nonlinear piezoelectric vibration energy harvesting circuit: Mechanisms, effects, and solutions," *IEEE Trans. Power Electron.*, vol. 34, no. 3, pp. 2427–2440, Mar. 2019.

[17] E. E. Aktakka and K. Najafi, "A micro inertial energy harvesting platform with self-supplied power management circuit for autonomous wireless sensor nodes," *IEEE J. Solid-State Circuits*, vol. 49, no. 9, pp. 2017–2029, Sep. 2014.

[18] S. Saggini, S. Giro, F. Ongaro, and P. Mattavelli, "Implementation of reactive and resistive load matching for optimal energy harvesting from piezoelectric generators," in *Proc. IEEE 12th Workshop Control Model. for Power Electron.*, 2010, pp. 1–6.
[19] L. Costanzo, A. L. Schiavo, and M. Vitelli, "Active interface for piezoelectric harvesters based on multi-variable maximum power point tracking," *IEEE Trans. Circuits Syst. I, Reg. Papers*, vol. 67, no. 7, pp. 2503–2515, Jul. 2020.
[20] Z. Chen, M. Law, P. Mak, W. Ki, and R. P. Martins, "Fully integrated Inductor-less flipping-capacitor rectifier for piezoelectric energy harvesting," *IEEE J. Solid-State Circuits*, vol. 52, no. 12, pp. 3168–3180, Dec. 2017.
[21] S. Du, Y. Jia, C. Zhao, G. A. J. Amaratunga, and A. A. Seshia, "A fully integrated split-electrode SSHC rectifier for piezoelectric energy harvesting," *IEEE J. Solid-State Circuits*, vol. 54, no. 6, pp. 1733–1743, Jun. 2019.
[22] A. Romani, M. Filippi, and M. Tartagni, "Micropower design of a fully autonomous energy harvesting circuit for arrays of piezoelectric transducers," *IEEE Trans. Power Electron.*, vol. 29, no. 2, pp. 729–739, Feb. 2014.
[23] A. Shareef, L. Wang, Y. Gao, and N. Srikanth, "A Rectifier-less AC–DC interface circuit for ambient energy harvesting from low-voltage piezoelectric transducer array," *IEEE Trans. Power Electron.*, vol. 34, no. 2, pp. 1446–1456, Feb. 2019.
[24] M. Meng, "Multi-beam shared-inductor reconfigurable voltage/sece-mode piezoelectric energy harvesting of multi-axial human motion," in *Proc. IEEE Int. Solid-State Circuits Conf.*, Feb. 2019, pp. 426–428.
[25] X. Wang, Y. Xia, G. Shi, H. Xia, Y. Ye, and Z. Chen, "Extensible multi-input synchronous electronic charge extraction circuit based on triple stack resonance for piezoelectric and thermoelectric energy harvesting," *IEEE Trans. Ind. Electron.*, early access, Jun. 2020, doi: 10.1109/TIE.2020.3001814.
[26] S. Chamanian, H. Ulusan, A. Koyuncuoglu, A. Muhtaroglu, and H. Kulah, "An adaptable interface circuit with multi-stage energy extraction for low power piezoelectric energy harvesting MEMS," *IEEE Trans. Power Electron.*, vol. 34, no. 3, pp. 2739–2747, Mar. 2019.
[27] T. Hehn *et al.*, "A fully autonomous integrated interface circuit for piezoelectric harvesters," *IEEE J. Solid-State Circuits*, vol. 47, no. 9, pp. 2185–2198, Sep. 2012.

Zhidong Chen received the B.E. degree in electronic and information engineering and the M.S. degree in electronic circuit and system from Hangzhou Dianzi University, Zhejiang, China, in 2011 and 2014, respectively. He is currently working toward the Ph.D. degree with Ningbo University, Ningbo, China.

He is currently a Lecturer with Zhejiang Business Technology Institute, Ningbo, China. His research interests include energy harvesting systems, sensors, and measuring technology.

Yinshui Xia (Member, IEEE) received the B.S. degree in physics and the M.S. degree in electronic engineering from Hangzhou University, Zhejiang, China, in 1984 and 1991, respectively, and the Ph.D. degree in electronic engineering from Edinburgh Napier University, Edinburgh, U.K., in 2003.

He was a Visiting Scholar with King's College London in 1999 and then joined Edinburgh Napier University as a Research Assistant and Research Fellow from 2000 to 2005. He is currently a Professor with Faculty of Electrical Engineering and Computer Science, Ningbo University, Ningbo, China. His research interests include low-power digital circuit design, logic synthesis and optimization, system on chip (SoC) design, and energy harvesting systems.

Ge Shi received the B.E. degree in electrical engineering and automation and the M.S. degree in detection technology and automation from China Jiliang University, Zhejiang, China, in 2004 and 2010, respectively, and the Ph.D. degree in micro–nano information system from Ningbo University, Ningbo, China, in 2018.

He is a Senior Experimentalist with China Jiliang University, Hangzhou, China. His research interests include energy harvesting systems, sensors and measuring technology, ultralow power ICs design, as well as embedded system.

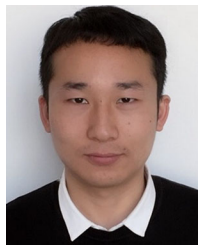

Xiudeng Wang (Student Member, IEEE) received the B.S. degree in communication engineering and the M.S. degree in electronic circuit and system in 2016 and 2019, respectively, from Ningbo University, Ningbo, China, where he is currently working toward the Ph.D. degree in electronic science and technology.

His research interests include energy harvesting systems, sensors, and measuring technology, ultralow power ICs design, as well as embedded system.

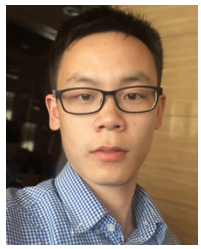

Huakang Xia received the B.E. degree in aircraft design and engineering and the Ph.D. degree in instrument science and technology from Nanjing University of Aeronautics and Astronautics, Nanjing, China, in 2012 and 2017, respectively.

He is currently a Lecturer with the Faculty of Electrical Engineering and Computer Science, Ningbo University, Ningbo, China. His current research interests include energy harvesting system, ultra-low power circuit design, as well as embedded system.

Yidie Ye (Member, IEEE) received the B.E. degree in electronic engineering and the Ph.D. degree in circuits and systems from Zhejiang University, Hangzhou, China, in 2007 and 2012, respectively.

She is currently a an Assistant Professor with the Faculty of Electrical Engineering and Computer Science, Ningbo University, Ningbo, China. Her current research interests include low-power circuit design and optimization.